The Geological Society of America | American Geophysical Union
Special Paper 514 | Special Publication 71
2015

The upper mantle geoid: Implications for continental structure and the intraplate stress field

David Coblentz*
Geophysics Group, Los Alamos National Laboratory (LANL), Mailstop F665, Los Alamos, New Mexico 87545, USA

Jolante van Wijk
Department of Earth and Environmental Science, New Mexico Institute of Mining and Technology, Socorro, New Mexico 87545, USA

Randall M. Richardson
Department of Geosciences, University of Arizona, Tucson, Arizona 85721, USA

Mike Sandiford
School of Earth Sciences, University of Melbourne, Melbourne, VIC 3010, Australia

ABSTRACT

We use the fact that geoid anomalies are directly related to the local dipole moment of the density-depth distribution to help constrain density variations within the lithosphere and the associated tectonic stresses. The main challenge with this approach is isolating the upper mantle geoid contribution from the full geoid (which is dominated by sources in the lower mantle). We address this issue by using a high-pass spherical harmonic filtering of the EGM2008–WGS 84 geoid to produce an "upper mantle" geoid. The tectonic implications of the upper mantle are discussed in terms of plate tectonics and intraplate stresses. We find that globally there is a ~9 m geoid step associated with the cooling oceanic lithosphere that imparts a net force of ~2.5×10^{12} N/m in the form of "ridge push"—a magnitude that is consistent with one-dimensional models based on first-order density profiles. Furthermore, we find a consistent 6 m geoid step across passive continental margins which has the net effect of reducing the compressive stresses in the continents due to the ridge push force. Furthermore, we use the upper mantle geoid to reevaluate the tectonic reference state which previous studies estimated using an assumption of Airy-based isostasy. Our evaluation of the upper mantle geoid confirms the near-equivalence of the gravitational potential energy of continental lithosphere with an elevation of ~750 m and the mid-ocean ridges. This result substantiates early conclusions about the tectonic reference state and further supports the prediction that continental regions are expected to be in a slightly extensional state of stress.

*Corresponding author; coblentz@lanl.gov

Coblentz, D., van Wijk, J., Richardson, R.M., and Sandiford, M., 2015, The upper mantle geoid: Implications for continental structure and the intraplate stress field, *in* Foulger, G.R., Lustrino, M., and King, S.D., eds., The Interdisciplinary Earth: A Volume in Honor of Don L. Anderson: Geological Society of America Special Paper 514 and American Geophysical Union Special Publication 71, p. 197–214, doi:10.1130/2015.2514(13).

INTRODUCTION

Much of Don Anderson's scientific research addressed how plate tectonics is related to mantle convection. He was a strong advocate of "top-down tectonics" (Anderson, 2001), a system in which the tectonic plates organize mantle convection, not vice-versa as is generally advocated in the conventional view of plate tectonics (i.e., the lithosphere is simply the surface boundary layer of mantle convection). In this contribution we explore what geodynamic insights can be gleaned from an evaluation of the upper mantle geoid, which provides information about the density distribution with depth. It is our hope that an examination of the geoid from the "top down" will provide a perspective on the tectonic implications of the upper mantle density distribution—an approach that we feel that Don Anderson certainly would have advocated.

Evaluation of the geoid provides a way to understand the distribution of density contrast with depth in the Earth. This is a relevant approach for addressing the geodynamics and intraplate stress field, given the fact that the relationship between the gravitational potential energy (GPE) associated with lithospheric density contrasts and the dynamics of lithospheric deformation is well established (Artyushkov, 1973; England and Houseman, 1988; Fleitout and Froidevaux, 1982; Frank, 1972; Houseman et al., 1981; Lister, 1975; Molnar and Tapponier, 1978; Ricard et al., 1984) and can be related directly to the source of tectonic stresses responsible for sedimentary basin development, mountain-building processes, and continental deformation (Naliboff et al., 2009, 2011).

Initial studies of lithospheric GPE assumed Airy isostasy to estimate the lithospheric density distribution (Coblentz et al., 1994; Coblentz and Sandiford, 1994; Ghosh et al., 2009; Jones et al., 1996, Sandiford and Coblentz, 1994; Sandiford and Powell, 1990; Zhou and Sandiford, 1992). While this assumption was adequate for establishing the first-order GPE estimates, it is clear that assumption of pure-Airy compensation is an oversimplification, particularly for the continental lithosphere, and it is timely to reevaluate plate-scale estimates of the GPE, using the geoid filtered to extract the upper mantle contribution.

It is now clear that a simple relationship does not exist between the surface elevation of continental lithosphere and crustal thickness variations, a notion articulated by a number of recent studies. Zoback and Mooney (2003) evaluated lithospheric buoyancy and structure and concluded that elevations based on purely crustal buoyancy (i.e., Airy isostasy) commonly exceed observed elevations. Furthermore, their results indicate that the magnitude of the compressive stresses in the continents (due to far-field tectonic forces) is generally lower than previously assumed, and the potential energy of lithospheric roots has a significant influence on the state of stress (generally resulting in more compression in cratonic regions). Seismic tomography studies indicate that the topography of the Southern Rocky Mountains (western U.S.) has a significant component of dynamic support from the upper mantle (Coblentz et al., 2011; Karlstrom et al., 2012). There is a growing body of evidence that Neogene and ongoing upper mantle convection is driving surface uplift of the Colorado Plateau region (western U.S.) (Crow et al., 2011; Karlstrom et al., 2007, 2008; Levander et al., 2011; Liu et al., 2011; Liu and Gurnis, 2010; Moucha et al., 2009; van Wijk et al., 2010). Furthermore, it appears that thermal expansion is an important mechanism for topographic support of the North American Cordillera (Hyndman and Currie, 2011). Simple isostatic arguments show that the assumption of Airy compensation with pure crustal thickening can significantly underestimate the lithospheric GPE (Sandiford and Powell, 1990). It is now recognized that the assumption of Airy isostasy provides an inadequate base to estimate GPE and may in fact introduce a significant bias in comparison between continental and oceanic realms (Coblentz et al., 2011; Karlstrom et al., 2012), which has important consequences for estimates of the global distributions of GPE and the structure and evolution of the continents (e.g., Sandiford, 2010).

Here we take the approach of revising the estimate of the plate-scale GPE using harmonic filtering to isolate the upper mantle geoid signal from the full geoid field (which, because of the large-amplitude low-order terms, is likely dominated by signals originating in the lower mantle). In the absence of direct measurement of geometry and density distribution (which is available only in limited areas), the upper mantle geoid provides information about the distribution of density with depth in the lithosphere and allows an estimate of the lithospheric GPE. To a good approximation (within the limit of long wavelength and isostatic compensation), the geoid anomaly caused by density variations above the depth of compensation is proportional to both the vertical dipole moment of the mass distribution above the depth of compensation (Haxby and Turcotte, 1978) and the lithospheric GPE:

$$\Delta N = \frac{2\pi G}{g}\int_S^D z\Delta\rho(z)dz = \frac{(2\pi G)U_l}{g^2}, \quad (1)$$

where ΔN is the geoid anomaly; G, Newton's gravitational constant; g, the value of gravitational acceleration on the reference ellipsoid; D, the depth of compensation (the depth below geoid at which pressure becomes equal beneath columns in isostatic balance, or here, where lateral density differences cease); S, the surface elevation; z, the depth; $\Delta\rho(z)$, the lateral difference in density from a reference lithosphere, including crust; and U_l, the GPE of the lithosphere. An important consequence of the direct relationship between the GPE and the geoid is that Equation 1 provides a way to estimate the GPE without assumptions about the compensation mechanism. In particular, using the upper mantle geoid in Equation 1 allows the GPE to be evaluated in elevated continental regions (e.g., the western U.S.) where simple Airy-type compensation is not a valid assumption.

In the analysis below, we use the Earth Gravitational Model 2008 (EGM2008) (Pavlis et al., 2012), which has recently been released by the U.S. National Geospatial-Intelligence Agency and provides the Earth's gravitational model complete to spherical

harmonic degree and order 2159. We present the upper mantle geoid derived from EGM2008 and discuss a number of tectonic implications for the lithospheric reference state.

THE EARTH'S GEOID FIELD

The geoid is defined as the equipotential surface of the Earth's gravity field that best fits (in a least-squares sense) the global mean sea level. As such, the Earth's geoid is the volumetric integrated mass distribution, and the geoid alone cannot be used to evaluate lateral density. However, additional (and independent) geophysical information can be used to interpret the geoid in terms of the lateral density variations in the lithosphere responsible for convection, plate tectonics, surface topography, and intraplate stresses (Chapman, 1979; Chase, 1979, 1985; Hager, 1983; Kaula, 1967; Vanicek and Christou, 1994). One such approach is to use the ratio of the geoid anomaly to topography (at wavelengths greater than the flexural wavelength) to estimate the depth of compensation of crustal plateaus and the depth of compensation of hotspot swells (Chase et al., 2002; Coblentz et al., 2007, 2011; Cserepes et al., 2000; Haxby and Turcotte, 1978; Sandwell and Mackenzie, 1989; Sandwell and Renkin, 1988; Watts et al., 2006).

Satellite data are typically used to compute spherical harmonic coefficients C_{nm} and S_{nm} for the harmonic expansion of the geoid:

$$N(\phi,\theta) = \frac{GM}{R}\frac{1}{g_o}\sum_{n=2}^{\infty}\sum_{m=0}^{n}\left(\frac{a_e}{R}\right)^n [C_{nm}\cos m\theta + S_{nm}\sin m\theta]\, P_{nm}(\sin\phi), \quad (2)$$

where M and R are the mass and radius of the Earth, respectively; a_e is the Earth's equatorial radius; and g_o is normal gravity acceleration. The arguments ϕ and θ are the geocentric co-latitude and longitude, respectively, at the location of the calculation; C_{nm} and S_{nm} are the fully normalized spherical harmonic coefficients of degree n and order m, referenced to an ellipsoid Earth; and P_{nm} is the associated Legendre polynomials (Bowin, 2000b).

The Earth's geoid height anomaly (relative to the World Geodetic System [WGS] 84 ellipsoid) based on the EGM2008 model (degree and order up to 2159) is shown in Figure 1A. This geoid anomaly is the height above or below the chosen reference ellipsoid, so the polar flattening and equatorial bulge (ellipticity) of the geoid doesn't show in Figure 1A because this field is the difference between a (near) ellipsoidal geoid and a reference ellipsoid (effectively, the J1 and J2 terms in the expansion of the gravitational potential). As pointed out by Anderson (1982) and others, the geoid anomalies in Figure 1A do not correlate well with the present-day tectonic features of the Earth (with the exception of the trenches and hotspots). Most of the power in the Earth's geoid can be explained in terms of lower mantle structure imaged by seismic tomography (Hager et al., 1985; Hager and Richards, 1989; King and Masters, 1992; King, 1995; Mitrovica and Forte, 1997; Forte and Mitrovica, 2001), with 75% of the signal produced by degree and order terms 2 and 3. It is clear that the Earth's geoid is dominated by long-wavelength, high-amplitude anomalies that arise from deep mantle density heterogeneities (Hager and Richards, 1989), with the source of the very long-wavelength geoid (degree and order <5) thought to be controlled by topographic relief of <3 km at the core-mantle boundary (Bowin, 1986). Removal of the signal from subducted slabs (Chase, 1979; Crough, 1979; Crough and Jurdy, 1980; Kaula, 1967; Hager, 1983) demonstrates that this residual geoid is characterized by two dominant mass anomalies in the deep mantle near the core-mantle boundary (Becker and Boschi, 2002). Apart from the geoid highs associated with subduction zones along the western Pacific Rim, there is little correlation between the geoid and surface features such as continents (with the notable exception of the Andes) and mid-ocean ridges (Kaula, 1967). As pointed out in previous studies (e.g., Vanicek and Christou, 1994), large-scale lithospheric features such as the continental land masses and ocean basins are not prominent features in the global geoid field. We also note that Anderson (1982) speculated that many aspects of continental geology (particularly the distribution of Cretaceous volcanism) can be related to the insulation properties of the continents as they move over more stationary geoid highs.

There are, however, large variations between the geoid values for the ridges, oceanic basins, and continental regions for the individual plates. There is nearly 30 m difference between the continents characterized by positive average geoid anomaly (Africa, +16 m; Australia, +17.4 m) and the continents characterized by negative average geoid anomaly (North America, –14 m; Eurasia, –10.4 m). This large degree of intercontinental variation is characteristic of the long-wavelength geoid and far exceeds the plausible lithospheric contributions to geoid anomalies (as discussed below, the variation in the upper mantle geoid is much less) and therefore reflects deeper mantle contributions. We further note that geoid gradients across individual continents can be significant—for example, geoid variations across the continent of Australia are in excess of 30% of the total global geoid range. We note that the zero geoid anomalies (designated by the black contour line in Fig. 1B) correlate quite well with the coastlines of the continents. Thus, while there is general agreement that the geoid is dominated by the density structure of subducted slabs and lower mantle structure, our understanding of the contribution to the geoid from upper mantle and lithospheric sources is less complete.

The correlation between the global distribution of hotspots (Anderson and Schramm, 2005) and the full geoid field is weak; however, most hotspots are located in regions of positive geoid anomaly (Chase, 1985; Crough and Jurdy, 1980). The magnitude of the geoid anomaly associated with individual hotspots varies greatly (+9 m for Yellowstone, +20 m for Hawaii, and +60 m for Iceland). In the residual geoid field used by Crough and Jurdy (1980), this difference is just as large (with residual geoid values of ~–15 m for Yellowstone, +40 m for Hawaii, +25 m for Iceland). In general, however, a direct relationship between the long-wavelength (complete or residual) geoid and hotspots remains ambiguous.

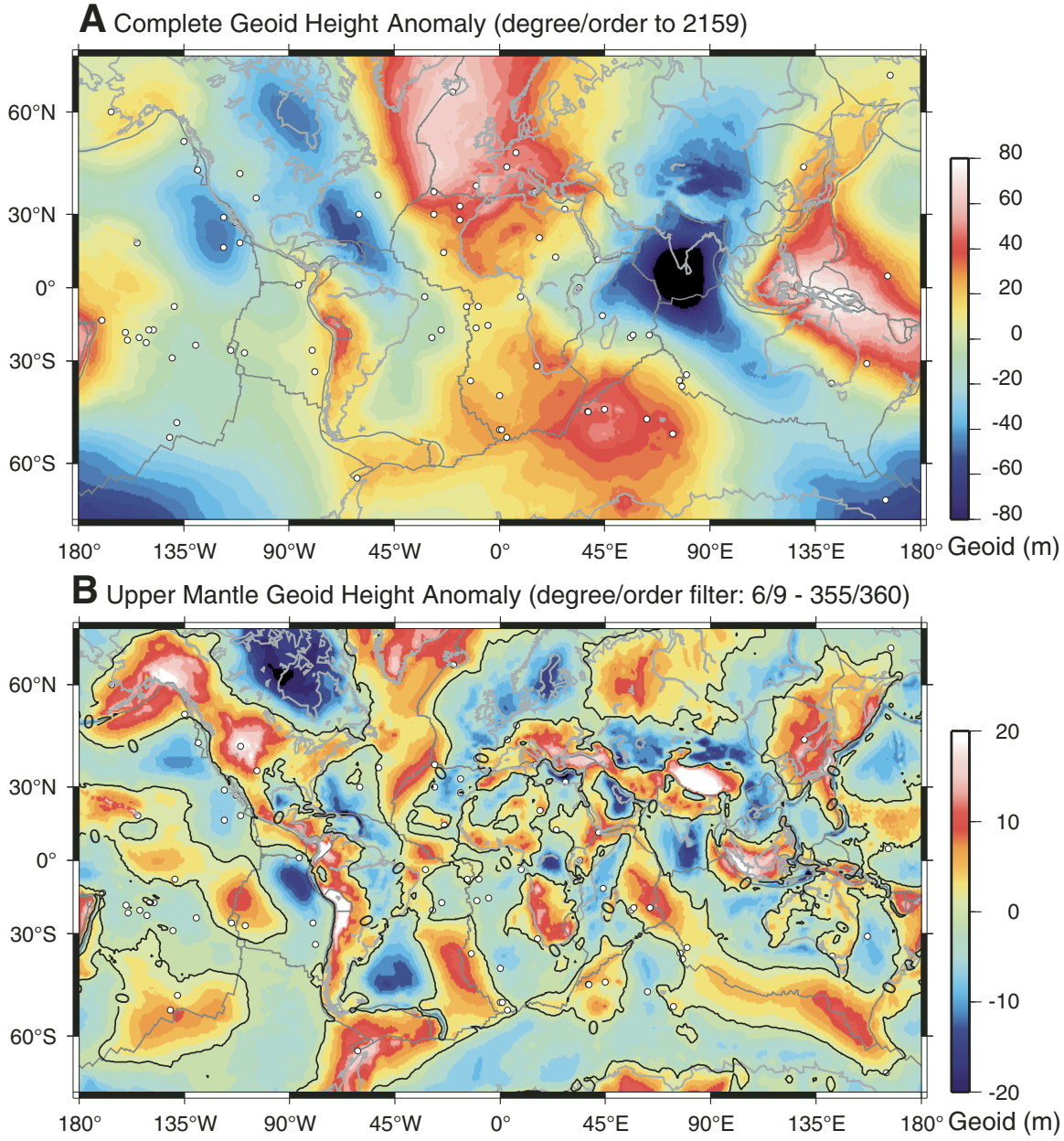

Figure 1. (A) Complete (unfiltered) geoid height anomaly, relative to the WGS 84 ellipsoid, based on the EGM2008 model (degree and order up to 2159). (B) Upper mantle geoid anomaly derived from a harmonic filter passing coefficients between degree and order 9 and 355 with a cosine taper between both degree and order 6 to 9 and 355 to 360. See text for details. Black contour line designates an upper mantle geoid height of 0 m; note that this contour is roughly conformal to sea level for the continents. Open circles are hotspot locations (Anderson and Schramm, 2005).

THE UPPER MANTLE GEOID

Given the dominance of the full geoid field by deep sources in the Earth, an evaluation of the geoid signal arising from lithospheric sources would be a more productive way of discerning the relationship between the geoid (and, by extension, GPE) and lithospheric tectonic processes. An evaluation of the geoid signal associated with density variations in the upper mantle requires the removal of the long-wavelength geoid signals arising from sources in the lower mantle. Here we generate an "upper mantle geoid" by filtering the spherical harmonic terms used in the harmonic expansion of the geoid to extract the geoid signal from the uppermost mantle density variations. We note at the outset of this evaluation that this approach relies on certain assumptions about the relationship between the degree and order of the spherical harmonic expansion terms and the source depth to separate the

upper mantle geoid anomalies from those with deeper sources. To a first order, the maximum depth of the causative mass can be expressed as a fraction of the Earth's radius (r), which corresponds to each spherical harmonic degree (n). The spherical harmonic degree also corresponds to the wavelength (λ) of geoid anomaly features at the Earth's surface such that the source depth (Z_n) for a particular degree and order can be expressed as (Bowin, 1983; Featherstone, 1997):

$$Z_n = \frac{r\lambda}{(360 - \lambda)}, \text{ where } \lambda = \frac{(360)}{n} \text{ in arc degrees.} \quad (3)$$

Inherent in Equation 3 is the assumption that low-degree (long-wavelength) components of the geoid originate from deep sources within the Earth and successively shorter wavelengths are added from increasingly shallower mass density anomalies. This relationship between depth and spherical harmonic degree does not preclude any contribution to the geoid anomaly from shallower sources due to the non-uniqueness of the geopotential field inversion. Therefore, Equation 3 provides only an upper depth limit of the mass anomaly. The issue of plausible source depths for the geoid remains contentious, with some evidence suggesting that long-wavelength geoid anomalies can be explained in terms of shallow (e.g., upper mantle and lithospheric) mass variations (Khan, 1977; Lambeck, 1988; Mishra and Kumar, 2012) and other studies suggesting that the geoid anomalies are purely depth dependent such that Equation 3 is appropriate for computing the source depth of the density variations responsible for the geoid (Allan, 1972; Bowin, 1983, 2000a, 2000b). Using this approach, the upper mantle geoid was generated by removing spherical harmonic terms of degree less than 6 and greater than 355, and applying a one-sided cosine taper to harmonic terms between degrees 6 and 9 and between 355 and 360 (Chase et al., 2002; Coblentz et al., 2007). Using Equation 3, this filter removes the contribution from harmonic components with spatial wavelengths greater than 3000 km and limits the sources of the anomaly to depths less than ~600 km. The filtering used to produce this geoid is nearly identical that used by Chase et al. (2002) to produce the "lithospheric" geoid. Because the source depth extends well into the upper mantle, we consider this filtered geoid to be more properly referred to as the "upper mantle geoid".

Whereas there is little correlation between the Earth's physiographic features and the full geoid, many of the Earth's tectonic features (both continental and oceanic) are evident in the upper mantle geoid (Fig. 1B). Qualitatively, there is a strong correlation between elevated continental regions and positive upper mantle geoid anomalies, particularly for the western U.S., the Andes, South Africa, and the Tibetan Plateau. Other continental regions have marked upper mantle geoid lows—most notably the Congo Basin, the Canadian Shield, and southern Australia.

Evaluation of the mean geoid anomaly values for the Earth's tectonic features provides a way to quantitatively assess the upper mantle geoid anomaly and its tectonic significance. A plot of the relationship between elevation and the complete geoid anomaly (Fig. 2A) substantiates the poor correlation between the complete geoid and the Earth's tectonic provinces. The scatter in the

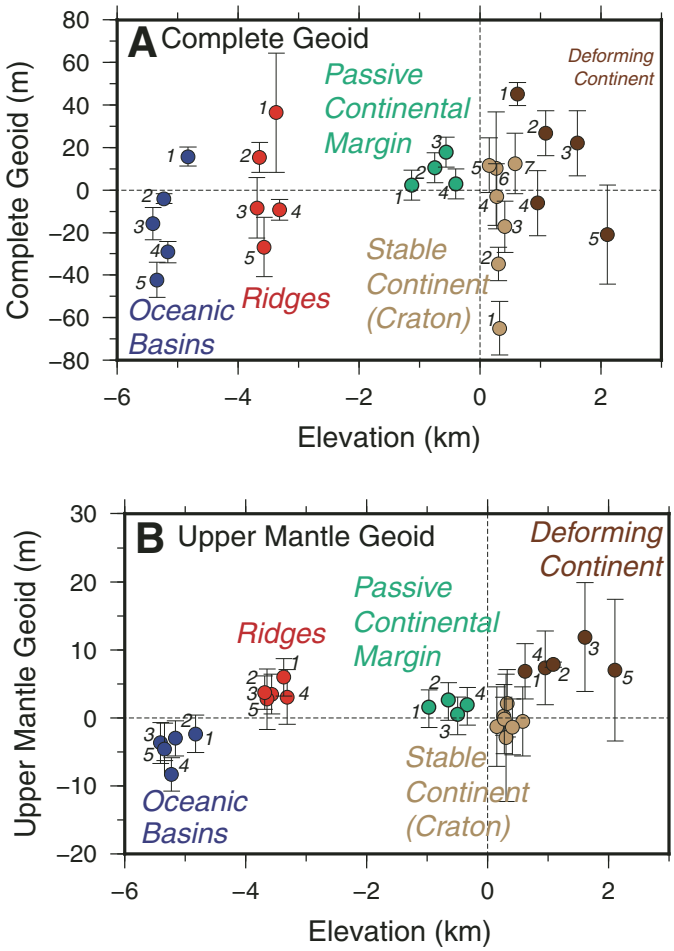

Figure 2. Correlation between elevation and the geoid anomaly for the complete geoid (A) and the upper mantle geoid (Fig. 1B) (B). Shown are the averages and one standard deviation about the mean for a number of locations within the oceanic basins (blue), mid-ocean ridges (red), passive continental margins (green), cratons (tan) (here defined as continental regions that have remained stable since the Archaean and the Proterozoic), and deforming continental regions (brown) (here defined as elevated continental lithosphere of Mesozoic–Cenozoic age; Prodehl and Mooney, 2012). Whereas there is considerable scatter within the four provinces from the complete geoid (A), the distributions for the upper mantle geoid (B) show a high degree of coherence. Numerical index: oceanic basins (1—Africa; 2—South Atlantic; 3—North Pacific; 4—southern Indian Ocean; 5—North Atlantic); ridges (1—northern Mid-Atlantic Ridge; 2—southern Mid-Atlantic Ridge; 3—Southeast Indian Ridge; 4—East Pacific Rise; 5—Southern East Pacific Rise); continental margin (1—North America; 2—Africa; 3—Indo-Australia; 4—South America); stable continental craton (1—India; 2—North America; 3—Siberia; 4—South America; 5—Australia; 6—Europe; 7—Africa); and deforming continent (1—Europe; 2—S. Southern Africa; 3—South America; 4—western North America; 5—Asia).

complete geoid anomaly for the areas considered in each of the four province types is significant, typically greater than 60 m. In contrast, the upper mantle geoid anomalies for the four tectonic provinces are much more tightly clustered (Fig. 2B). We note that the high average elevation of the Andean region of South America and the Tibetan Plateau in Asia breaks up the clustering of the deforming continental locations in an elevation framework.

Several general conclusions can be drawn from Figure 2B. The global average for stable near-sea-level continental regions (cratons) is very close to zero, implying a near-neutral potential energy state that supports the notion that near-sea-level continental lithosphere is a viable candidate for tectonic reference state (see further discussion on this topic below). The difference in the upper mantle geoid anomaly average for the mid-ocean ridges (~3 m) and the oceanic basins (~–5 m) indicates that, on average, the geoid drop from the ridge crest to the oceanic basins is ~8 m, corresponding to a decrease in the geoid anomaly with age for ocean lithosphere cooling over 84 m.y. of ~0.095 m/m.y. This geoid drop establishes a ridge push force of 2–3 × 10^{12} N/m that agrees well with numerical theory (e.g., see discussion in Turcotte and Schubert [2014]). The average upper mantle geoid anomaly for elevated, tectonically deforming continental lithosphere (~7 m) is nearly equivalent to the ridge–to–oceanic basin geoid drop, which has important tectonic implications. This equivalency demonstrates that, from a potential energy perspective, the compression in continental regions expected from the ridge push force can be counteracted by the extensional stresses generated by elevated and deforming continental lithosphere.

For illustrative purposes, the relationship between the upper mantle geoid and topography along two profiles is shown in Figure 3. Along both profiles, geoid anomalies greater than ~±10 m are significant departures from the mean. Some general observations for the oceanic regions include: (1) the upper mantle geoid anomaly corresponding to the northern Mid-Atlantic Ridge is in the range of 10–12 m, and that across the continental margins on both sides of the Atlantic is ~6 m, which is consistent with numerical predictions (e.g., Turcotte and Schubert, 2014); (2) there appears to be an inverse correlation between the spreading rate of the ridge axis and the magnitude of the upper mantle geoid anomaly, which is presumably related to the mantle dynamics at the ridge crests; and (3) while the geoid signature for the mid-ocean ridges can be as high as +15 m (e.g., across the northern Mid-Atlantic Ridge)—consistent with one-dimensional (1-D) models of the density distribution—we note that other ridge segments have considerably smaller geoid anomalies (e.g., the southern Mid-Atlantic Ridge along profile C-D). In the continental regions, the upper mantle geoid for stable cratonic regions approaches the average value for the mid-ocean ridges (within 1σ of the mean). Several continental features have large positive geoid signals that are of similar magnitude to those of the ridges—most proximately, Yellowstone, South Africa, the Andes, and the East African Rift. Stable cratonic regions along the profiles have a geoid anomaly generally less than 2 m. The upper mantle geoid for the major elevated continental plateaus (e.g., western U.S., Tibet, and South Africa) exceeds 10 m, consistent with the extensional stress state in these regions. The largest negative continental geoid anomaly is associated with the Congo Basin. That the Congo Basin contains the only compressional earthquakes in the continental interior of Africa (Delvaux and Barth, 2010; Craig et al., 2011) is evidence of the important role played by GPE in controlling stress regimes in the intra-continental regions. Finally, while some hotspots appear to be associated with distinct upper mantle geoid highs (e.g., Hawaii, Yellowstone, and Afar), others appear to be associated with broader geoid anomalies or have no apparent correlation with geoid anomalies. Iceland, for example, is part, but not the center, of the large North Atlantic geoid high. From a spectral perspective, the upper mantle geoid presented in Figure 1B highlights anomalies that have shorter-wavelength signal (both spatially and in depth) and are more likely to have their source in the upper mantle. It is possible that the mantle geoid anomalies may be indicative of small-scale convection in the upper mantle, which correlate with larger-scale, deeper convection associated with hotspots.

THE GEOID STEP ASSOCIATED WITH RIDGES AND CONTINENTAL MARGINS

An evaluation of the geoid step across the ridges and passive continental margins provides information about the GPE that generates intra-lithospheric tectonic forces and helps constrain the magnitude of the intraplate stresses. The geoid steps across 139 ridge profiles and 167 passive continental margin profiles for the upper mantle geoid (Fig. 4A) were extracted to determine the composite geoid step. Each ridge profile extends along both ridge flanks from the ridge crest to the 45 m.y. isochron about the ridges to capture as many ridges as possible globally, and hence as much oceanic lithosphere as possible. The continental margin profiles were constructed every 3° along passive continental margins worldwide, with each profile 10° in length, centered on the margin. The average geoid step associated with the ridges (Fig. 4B) is 4.5 m over the 45 m.y. interval, a step that is consistent with the ±10 m anomaly for the Atlantic over the 120 m.y. interval for a slowly spreading ridge, and corresponds to a ridge push force of 2–3 × 10^{12} N/m (consistent with the estimates of Haxby and Turcotte [1978]). The geoid step between the ridge crest and the oceanic basin (typically 80 m.y.) is therefore ~9 m—in good agreement with the global average step of 8 m shown in Figure 2. The composite average for the passive continental margins is

Figure 3. Topography of the Earth (A) and the upper mantle geoid (B) plotted with a Mollweide projection. The relationship between the topography and the upper mantle geoid along two profiles are shown in C and D. Profiles were chosen to follow great-circle paths that cross tectonic features of interest (ridges, hotspots, continental orogenic systems, passive continental margins, and basins). Upper mantle geoid values that exceed ±10 m are considered to be large anomalies for the purpose of comparison.

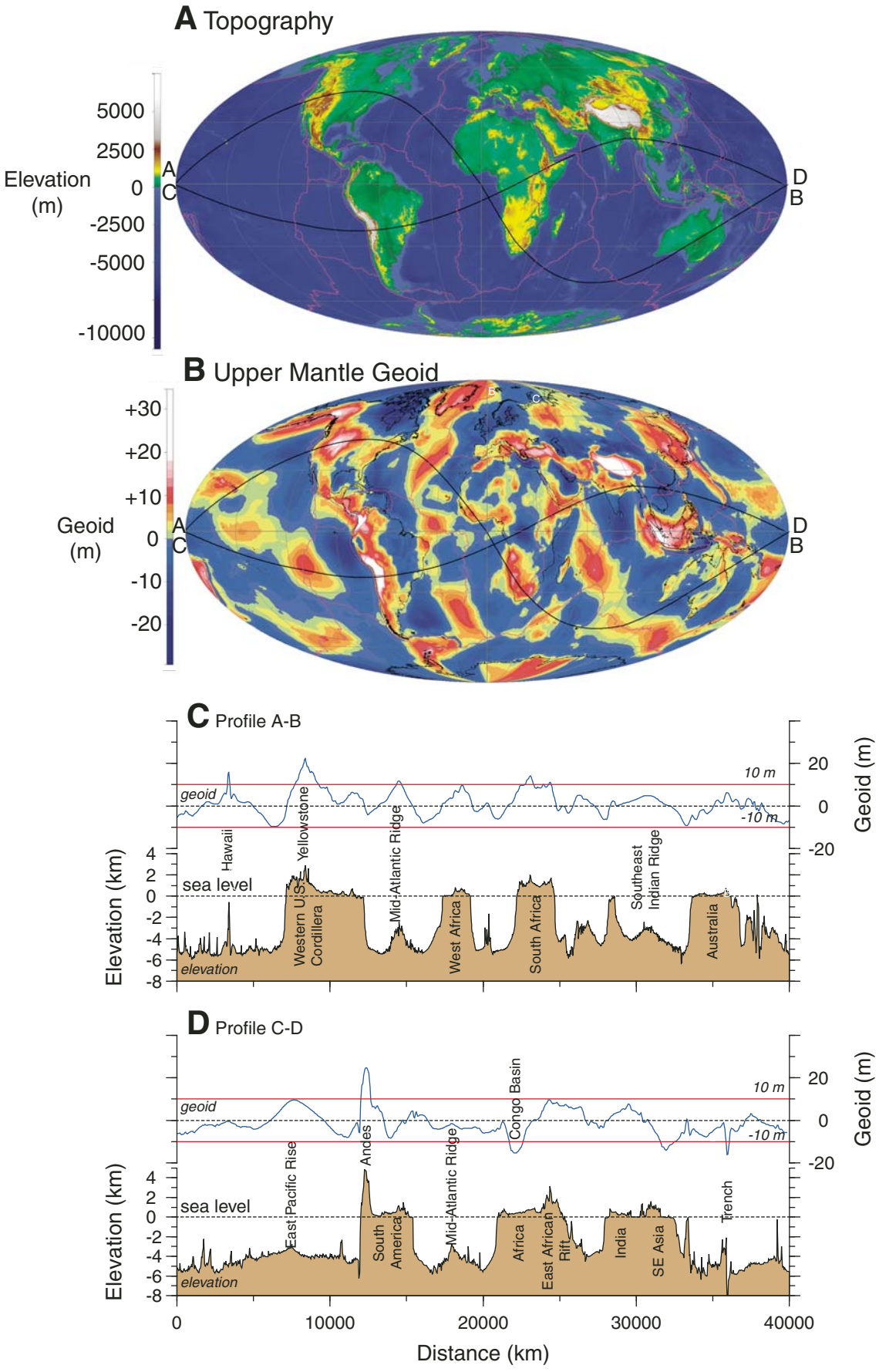
A Topography
Elevation (m)
5000
2500
0
-2500
-5000
-10000
A
C
D
B
B Upper Mantle Geoid
Geoid (m)
+30
+20
+10
0
-10
-20
C Profile A-B
geoid
10 m
-10 m
Geoid (m)
20
0
-20
Hawaii
Yellowstone
Mid-Atlantic Ridge
Southeast Indian Ridge
sea level
Western US Cordillera
West Africa
South Africa
Australia
elevation
Elevation (km)
4
2
0
-2
-4
-6
-8
D Profile C-D
Congo Basin
Andes
East Pacific Rise
Mid-Atlantic Ridge
South America
Africa
East African Rift
India
SE Asia
Trench
0
10000
20000
30000
40000
Distance (km)

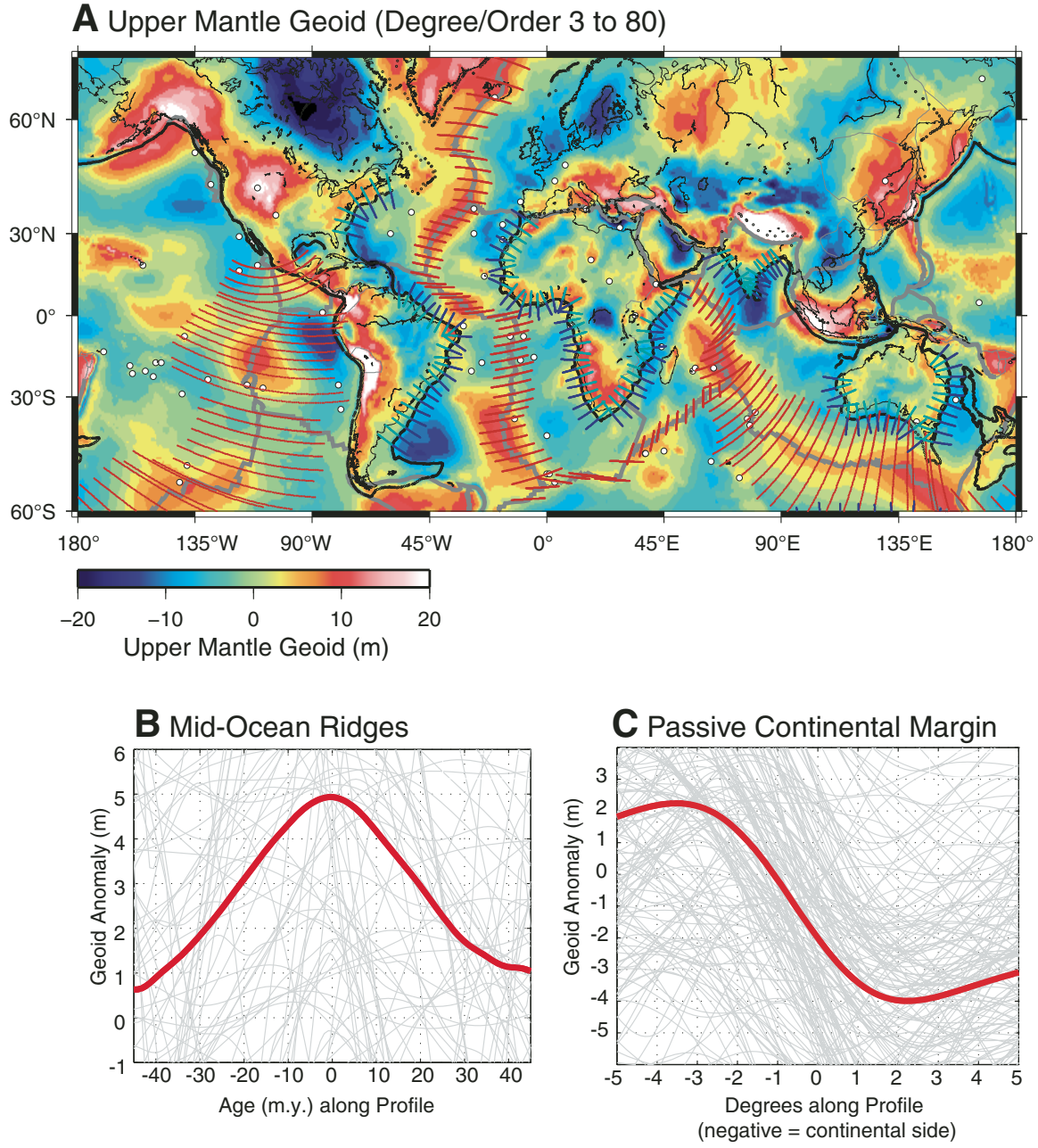

Figure 4. (A) Location of 139 ridge profiles (red; 48 in the mid-Atlantic, 9 in the South Atlantic, 48 in the Indian Ocean, and 34 in the Pacific Ocean) and 167 profiles located every 3° along passive continental margins worldwide (blue). The ridge profiles extend to ±45 m.y. so that data from different oceans can be combined. Each continental margin profile is 10° long, centered on the margin. (B, C) The composite step in the upper mantle geoid (here the geoid signal was passed for degree and order 3–80 to extract the long-wavelength signal) for the global ridges (B) and the continental margins (C). The gray-shaded lines illustrate the individual profiles, and the red line is the composite average. The global average geoid ridge anomaly is 4.5 m over ±45 m.y., consistent with the ±10 m anomaly for the Atlantic over ±120 m.y., corresponding to a ridge force of 2–3 × 10^{12} N/m. The average for the passive continental margins indicates a geoid anomaly of ~6 m.

~6 m (Fig. 4C), or about two-thirds of the ridge push potential energy step. These steps have the tectonic implication that for a typical continent, the compressional ridge push force generated by the cooling oceanic lithosphere will be significantly reduced by the extensional stresses generated by the density anomaly associated with the passive continental margins. We note there is considerable scatter in the individual profiles (the light gray lines shown in Figs. 4B and 4C), which reflects the fact that ridge and passive continental margin anomalies in the upper mantle geoid are not uniform along the ridge crest or margin boundary. For example, pronounced asymmetry is present along both the northern and the southern Mid-Atlantic Ridge. Clearly other long-wavelength density anomalies (possibly as shallow as 200 km; see discussion in French et al. [2013]) are influencing the upper mantle geoid signal.

COMPARISION WITH THE COOLING OCEANIC LITHOSPHERE MODEL

In the plate tectonics paradigm, the lithospheric plates are the surface manifestation of large-scale flow in the mantle, with convection of the mantle primarily controlled by thin thermal boundary layers (Turcotte and Oxburgh, 1967). Plate tectonics has seen its greatest success in the explanation of the thermal evolution and dynamics of the oceanic plates. To a very good approximation the bathymetry of the ocean floors increases with the square root of the age of the ocean floor (at least for ocean lithosphere younger than ca. 80 Ma), and the corresponding decrease in the heat flow with the square root of age gives rise to the well-established age–bathymetry–heat flow relationship for the cooling oceanic lithosphere. The density structure of the cooling oceanic plate can be computed using observed seafloor depth, surface heat flow, and geoid height data (see detailed discussions in Parsons and Sclater [1977], Stein and Stein [1992], McKenzie et al. [2005], and Grose and Afonso [2013]), and provides a way to compute the resulting "ridge push" force with a high degree of fidelity. The computed geoid derived from the cooling oceanic plate model (using the physical parameters from the GDH1, a cooling plate model defined by Stein and Stein, 1992) and the global crustal age data is shown in Figure 5A. The geoid drop from the ridge crest to the deep oceanic basin is ~12 m with gradients correlating with spreading rate (e.g., steeper gradients along the Mid-Atlantic Ridge as compared to the Indian Ocean ridges (Central Indian, SW Indian, and SE Indian Ridges) and the East Pacific Rise. For comparison, the upper mantle geoid for the oceanic regions is shown in Figure 5B. Whereas the geoid associated with the cooling plate model is uniform along the ridge crests, the upper mantle geoid exhibits a large number of long-wavelength features along the ridge segments that reflect upper mantle density variations and are presumably associated with upper mantle convection. There is good agreement between the two geoid fields (Fig. 5C) along many ridge segments, including the Southeast Indian Ridge, the southern Mid-Atlantic Ridge below ~40°S, most of the African plate ridge system, and along the northern Mid-Atlantic Ridge north of 45°N. The difference between the cooling oceanic plate geoid and the upper mantle geoid is large along many other ridge segments. For example, along most of the East Pacific Rise, the upper mantle geoid is almost 10 m less than the geoid derived from the cooling oceanic plate model. Similarly, along the northern Mid-Atlantic Ridge at 35°N and the southern Mid-Atlantic Ridge around 40°S, the difference approaches +5 m. There is generally good agreement between the two geoid fields throughout the deep ocean basins (except at hotspot locations, such as Hawaii, where the difference between the two geoid fields is as great as 12 m). In contrast to other oceanic areas, the geoid height in the southeastern Pacific does not appear to decrease with age with a small drop (<2 m)—a feature noted by Sandwell and Schubert (1980), among others. We note that the geoid differences shown in Figure 5C have a long spatial wavelength (generally >5000 km) suggesting that the source is widely distributed in the upper mantle. We note that the geoid is well resolved at these wavelengths (with the signal not "smeared" or distorted such that features would be better defined at higher resolutions).

IMPLICATIONS FOR THE AMBIENT STATE OF STRESS IN THE CONTINENTS

The African plate provides an ideal location to evaluate the ambient lithospheric state of stress in a continental plate, given its unique boundary geometry of being nearly completely surrounded by mid-ocean ridges (Coblentz and Sandiford, 1994). Evaluation of the state of stress in Africa is not complicated by boundary forces and is the product of upper mantle and lithospheric density forces arising from a combination of intraplate tectonic forces (e.g., ridge push from the cooling oceanic lithosphere) and basal tractions (e.g., upper mantle convection; see discussion in Lithgow-Bertelloni and Silver [1998] and Moucha and Forte [2011]). There is strong evidence that much of Africa's tectonic evolution (including the present-day high topography of the East African Rift and the South African plateau) is driven by buoyancy forces in the mantle (Lithgow-Bertelloni and Silver, 1998; Moucha and Forte, 2011), and examination of the upper mantle geoid can help refine our understanding of the density distributions responsible for this dynamic topography. The mean stress magnitudes (averaged over a 100-km-thick lithosphere) for the African plate are shown in Figure 6. The stresses were computed using a finite-element analysis of a lithospheric shell under traction from the GPE forces associated with the upper mantle geoid (see Coblentz and Sandiford [1994] and Humphreys and Coblentz [2007] for a discussion of the finite-element approach). For comparison, the average s_1 (maximum compressive stress) for three cases of the ridge push force formulation are considered: (1) a ridge crest boundary force of 2.5×10^{12} N per meter of ridge segment, (2) forces derived from the gradient in the geoid derived with the cooling oceanic lithosphere model (based on seafloor depth and crustal age data; Fig. 5A); and (3) forces derived from the gradient of the upper mantle geoid (Figs. 1B

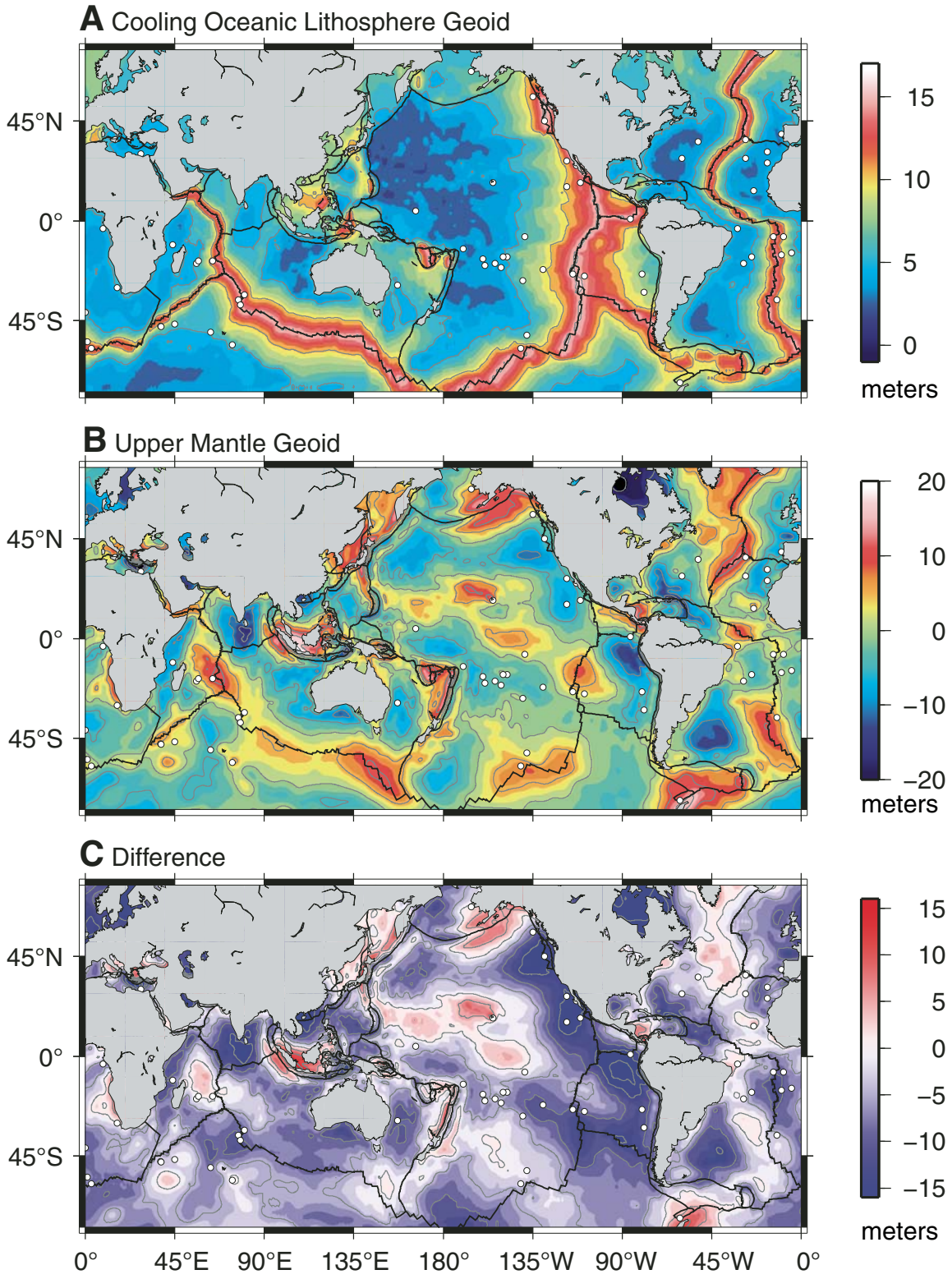

Figure 5. (A) Cooling oceanic lithosphere geoid derived from the thermal model discussed in the text. (B) Upper mantle geoid from Figure 1B. There is considerable variation in the geoid along the ridge crests and within the ocean basins indicative of complex upper mantle density anomalies. (C) Difference between A and B; red colors designate regions where the upper mantle geoid exceeds the geoid associated with the cooling oceanic lithosphere. The observed upper mantle geoid, while more complicated than the simple cooling plate geoid, still clearly shows a ridge signature. The long-wavelength differences from the simple cooling plate geoid are presumably associated with mantle convection.

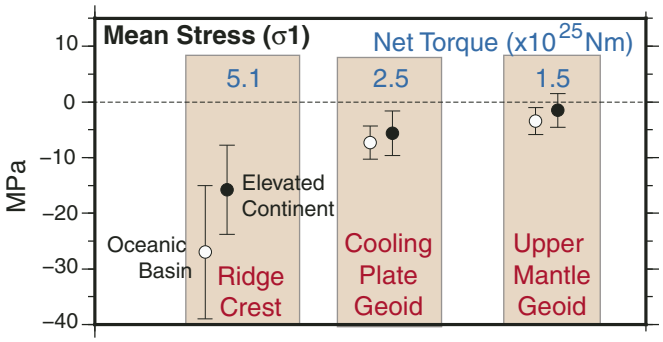

Figure 6. Mean σ_1 (maximum compressive stress) for three cases of the ridge push force formulation: (1) ridge crest boundary force of 2.5 × 10^{12} N/m; (2) gradient of the geoid derived from the cooling oceanic plate model; and (3) gradient of the geoid derived from the upper mantle geoid. Positive and negative mean stress magnitudes correspond to extension and compression, respectively. Error bars represent one standard deviation about the mean value. Blue numbers list the net torque acting on the plate for each case.

and 5B). The net torque acting on the plate for the geoid gradient formulations (1.5 and 2.5 × 10^{25} N·m) is less than half of the net torque for the ridge crest case (~5 × 10^{25} N·m), suggesting that the use of the upper mantle geoid to compute the ridge push force acting on the plate is more closely in a state of mechanical equilibrium (e.g., a near-zero net torque) and therefore more closely approximates the ambient state of stress. The ridge crest formulation is an oversimplification of the ridge push force (Richardson and Cox, 1984), and therefore the predicted magnitudes of σ_1 for this formulation (25 MPa in the oceanic basins and 15 MPa in the elevated continental regions) are overestimates of the compressive stress generated by the ridge push force. Computing the stresses using the geoid gradient is a way to reduce the uncertainty in estimating the density structure. Using this formulation, both the cooling oceanic plate model and the upper mantle geoid predict average compressive stresses in the range of 5–10 MPa in the oceanic basins, which are reduced by about a third in the continental regions. Ridge push based on the upper mantle geoid (which captures other subtleties in the upper mantle density structure that are difficult to explicitly include in a numerical model of the intraplate stress field) results in a predicted state of stress in the continental lithosphere that is neutral to slightly compressive and is more consistent with the observed intraplate stress field (e.g., Zoback and Mooney, 2003).

The fact that the ambient state of stress in the continental lithosphere is near neutral has important implications for understanding the sources of intraplate tension. This prediction differs significantly from other investigators' assumptions that the state of stress within the continents is dominated by stresses transmitted from the mid-ocean ridges and is therefore expected to be compressional with magnitudes in the range of 10–20 MPa averaged over the thickness of the lithosphere (e.g., Crough, 1983; Houseman and England, 1986; Zoback and Mooney, 2003). In the case of Africa, we find areas of high elevation and a thin mantle lid (East African Rift and South Africa) to be in a state of tectonic extension, which is consistent with the observed stress regime in these areas and indicative that the high elevations in Africa (and presumably elevated continental regions in other plates) are the result of density moments that exceed the potential energy of the surrounding mid-ocean ridges (Bird et al., 2006). Furthermore, we find that deviatoric stresses associated with upper mantle geoid (and therefore potential energy gradients) are in the range of 2–6 MPa—consistent with the recent work of Stamps et al. (2010, 2014) who found similar results using the thin viscous sheet approach for predicting the African intraplate stresses.

DENSITY SOURCES OF THE UPPER MANTLE GEOID

Given the important role that density variations in the uppermost mantle play in lithospheric geodynamics, it is of interest to constrain the depth of the density distributions that control the upper mantle geoid anomaly. The fact that the geoid height anomalies for isostatically compensated regions can be directly related to the local density dipole moment can be used to evaluate the subsurface distribution of mass associated with various surface features. Because the geoid anomaly reflects the gravitational dipole moment, it is more sensitive to deeper sources than the gravity field, a consequence of the fact that the geoid anomaly observed at the surface caused by a point mass buried at depth d decreases in amplitude as $1/d$, whereas the gravity anomaly of the same point mass decays as $1/d^2$. This relationship makes the study of geoid anomalies much more useful for evaluating the depth of isostatic compensation. The geoid anomaly has been used extensively in oceanic settings to evaluate the support mechanisms for oceanic plateaus and swells (Cserepes et al., 2000; Marks and Sandwell, 1991; Sandwell and Mackenzie, 1989; Sandwell and Renkin, 1988). On the continents, use of the geoid anomaly has seen somewhat fewer applications, in large part due to lack of a consensus on the basic physical processes responsible for the first-order density structure of continental crust (Brown and Rushmer, 2006), particularly when compared to the well-understood thermal-density evolution of oceanic lithosphere. Nevertheless, evaluation of the continental geoid anomaly has been used to deduce regional tectonic stresses from the variations of GPE (Coblentz et al., 1994; Jones et al., 1996; Sandiford and Coblentz, 1994; Sonder and Jones, 1999; Zhou and Sandiford, 1992) and to constrain deep continental structure as well (Doin et al., 1996; Ebbing et al., 2001).

One way to understand the source of the upper mantle geoid anomalies associated with tectonic features is to evaluate how individual harmonic degrees sum to form the total geoid anomaly. Following the approach of Bowin (1983, 2000a, 2000b), we use a modified cumulative contribution curve (CCC) to examine the relative degree and order contribution to the geoid anomaly. In the original formulation, the CCC curve for a given degree included the harmonic components for that degree and all lower degrees. Here, we compute the "cumulative reduction curve" (CRC), where the harmonic contribution for each degree is

computed as the total contribution from that degree up to degree 500. Essentially, the CRC approach works from the bottom up, progressively eliminating the contribution from lower degrees in the expansion. It is important to emphasize that the anomaly corresponding to a particular degree and order is not localized in any way. That is, the global geoid anomaly field for a given degree and order has been computed and the anomaly at a point of interest is evaluated to establish the point on the CRC curve. There is no spatial selection about the point of interest, and the long-wavelength information in the geoid anomaly field is preserved. The CRC curves for a number of tectonic settings are shown in Figure 7. A common feature of the CRC curves is the "red" character (greater spectral power at longer wavelengths) of the geoid anomaly power spectra (Bowin, 1983), with very large contribution to the geoid anomaly from low degrees (<10). Evaluation of the differences in the power spectra at mid-mantle depths (1000–600 km) for various tectonic settings provides a way to evaluate the density variations with depth beneath the locations. The salient conclusions that can be drawn from examination of Figure 7 include those below.

Hotspots and Plumes(?)

The relationship between mantle plumes and hotspots and the geoid anomaly remains contentious and the subject of considerable debate. Iceland, Yellowstone, and Hawaii are arguably the "classic" hotspots on Earth. The geoid anomalies associated with each of these three hotspots are, however, strikingly different: Iceland has a non-center location at the intersection of the North Atlantic geoid anomaly high and the spreading ridge (Fig. 1B); Yellowstone is centered in the geoid anomaly high of the North American plate, and the plume associated with Yellowstone is thought to have a profound influence on western U.S. tectonics (Parsons et al., 1994); and Hawaii is located at the tip of a lens-shaped geoid anomaly high in the Pacific plate. The CRCs shown in Figure 7A illustrate differences in the source depth of the upper mantle geoid anomaly between the three hotspots and provides a comparison with the "superplume" of South Africa. The harmonic degree contribution to the upper mantle geoid anomaly of Iceland is as might be as expected from a "classic" hotspot. Namely, the maximum geoid anomaly originates with the lowest harmonic degree and falls off rapidly with increasing harmonic degree. This character is suggestive of very deep density contrasts, presumably associated with the lower mantle origin of the geoid anomaly high in the North Atlantic. This contrasts with interpretations of tomographic images that show a strong low seismic–wave velocity anomaly only in the upper mantle below Iceland (Montelli et al., 2004), interpreted as an upper mantle origin of the Iceland melting anomaly. Both Yellowstone and Hawaii have an upper mantle geoid anomaly peak at a harmonic degree of 8, which corresponds to a source depth of ~900 km. This is consistent with studies of seismic wave velocity anomalies for Yellowstone that suggest the presence of a low-velocity anomaly at shallow upper mantle depths that is not imaged continuously into the deep mantle (Tian et al., 2009; Yuan and Dueker, 2005), and for Hawaii where the presence of low-velocity material has recently been imaged in the upper mantle below Hawaii and at mid-mantle depths west of Hawaii (Cao et al., 2011; Wolfe et al., 2009). We note that in contrast to Yellowstone, the Hawaiian hotspot has a significant geoid anomaly of 10 m (50% of the peak anomaly) up to harmonic degree 65 (which corresponds to a source depth of ~100 km). This is indicative of significant shallow density contribution to the Hawaiian geoid anomaly. The geoid anomaly associated with the African superplume—considered to be the largest discrete structure in the Earth's interior (Ni and Helmberger, 2003)—is about half the magnitude of that of the Hawaiian and Yellowstone hotspots and has a significant component in the lower and mid-mantle. This deep mantle source for the geoid anomaly is consistent with the interpretation that Southern Africa's high topography is dynamically supported by mantle flow induced by the density variations (Lithgow-Bertelloni and Silver, 1998; Bird et al., 2006). The other hotspots have little or no expression in the upper mantle geoid anomaly, supporting the notion that the Hawaii, Iceland, and Yellowstone hotspots are unique and are quite unlike the other global hotspots (King and Adam, 2014).

Continental Orogenic Systems

The harmonic distribution of the upper mantle geoid anomaly associated with the orogenic systems shown in Figure 7B is remarkably similar to that of the hotspots discussed above, and suggests that density variations associated with dynamic processes in the upper mantle have an important influence on the geoid anomaly. This is certainly true for the Southern Rocky Mountains, where Neogene mantle convection has driven long-wavelength surface deformation and uplift on the order of 500–1000 m, which may account for almost half of the current elevation of the region (Karlstrom et al., 2012). We note that the geoid anomaly for the Andes is similar in character to the Icelandic geoid anomaly and is consistent with very deep density sources. The lithospheric contribution to the geoid anomaly of the Andes is ~45 m, which corresponds to a very high geoid-to-elevation ratio of ~10 m/km that is indicative of dynamic support from sub-lithospheric sources such as mantle return flow (in this case, likely associated with the Nazca–South American subduction zone). The harmonic distribution below Tibet is negative in the range of ~30–60 degrees (shallow upper mantle), which likely reflects the subducted Indian plate that has been imaged in the upper mantle (Li et al., 2008; Zhang et al., 2014).

Continental Interiors

As discussed above, the upper mantle geoid anomaly is sensitive to mass variations at the base of the lithosphere (Doin et al., 1996), and a large geoid anomaly low is expected over continental shields. This is quantified in Figure 7C, which illustrates that the upper mantle geoid anomaly over cratonic regions can be

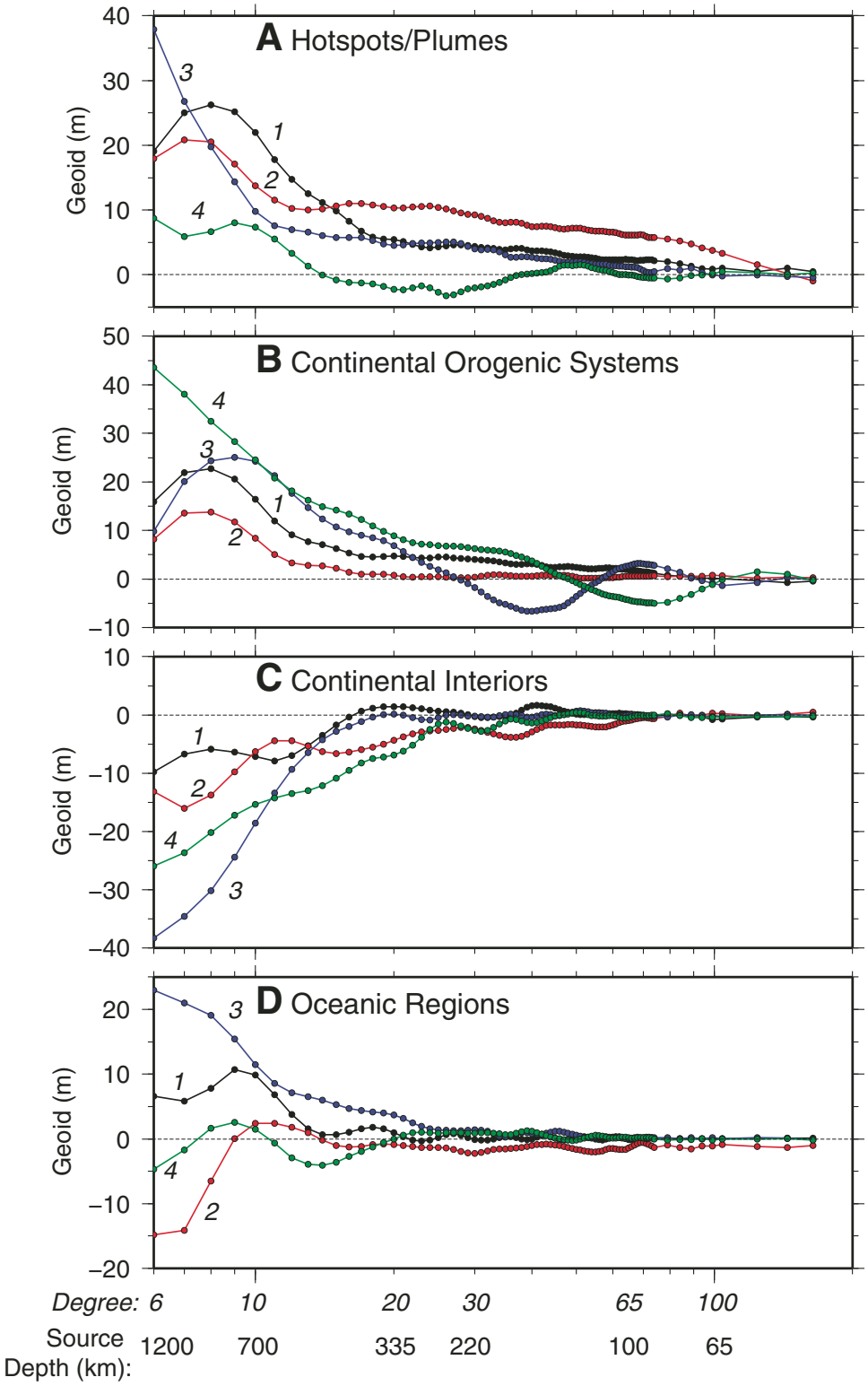

Figure 7. Upper mantle geoid cumulative reduction curves (CRC) for a number of hotspot (A), elevated plateau (B), continental interior (C), and oceanic regions (D) locations. As discussed in the text, the geoid for each spectral degree was computed for that degree to degree 500, effectively applying a high-pass filter to the geoid (Bowin, 2000a, 2000b). Italic numbers at the bottom of the figure indicate spectral degree and equivalent point source depth, respectively. Numerical index: hotspots/plumes (A: 1—Yellowstone; 2—Hawaii; 3—Iceland; 4—South Africa); continental orogenic systems (B: 1—Southern Rocky Mountains; 2—Colorado Plateau; 3—Tibet; 4—Andes); continental interiors (C: 1—Brazilian craton; 2—Central Australia; 3—North America; 4—Congo Basin); and oceanic regions (D: 1—East Pacific Rise; 2—Pacific Basin; 3—northern Mid-Atlantic Ridge; 4—Atlantic Basin).

as great as –40 m, as in the case of North America where a large negative anomaly at mid- to lower mantle depths is associated with the sinking Farallon slab. The Congo Basin (along with the Tarim Basin in Asia) has the most negative upper mantle geoid anomaly observed in the continental interiors. The Congo Basin is a deep cratonic basin, with sediment thicknesses up to 9 km (Laske and Masters, 1997). Its origin is debated (Buiter et al., 2012), and models for its formation include slow rifting (Crosby et al., 2010; Kadima et al., 2011), dynamic topography caused by a high-density lithospheric body (Downey and Gurnis, 2009), and upper mantle flow processes (Burke et al., 2008; Crosby et al., 2010; Forte et al., 2010; Moucha and Forte, 2011). We note that the upper mantle geoid anomaly of the Congo Basin has significant spectral power up to degree 20. This evidence for a strong source from shallower depths suggests a significant contribution from density variations associated with downwelling in the upper mantle (Moucha and Forte, 2011).

Oceanic Regions

The contrast in the upper mantle geoid anomaly between the mid-ocean ridge crest and the deep ocean basin for both the North Atlantic and the Pacific is illustrated in Figure 7D. In both cases, the difference in the geoid anomaly between the ridge and oceanic basin is in the range of 15–25 m, consistent with the 10 m predicted by 1-D estimates (Turcotte and Schubert, 2014). As noted by Turcotte and McAdoo (1979), the upper mantle geoid anomaly of the oceanic basins is comparable to that of the continental cratons, although the spectral power of the oceanic geoid anomaly attenuates at low harmonic degree (~10) in comparison to the continental cratons. We note the strong correlation between ridge spreading rate and the degree and order of the contribution to the geoid anomaly signal. Specifically, the geoid anomaly along the slow-spreading northern Mid-Atlantic Ridge has a larger contribution from lower degrees and orders as compared to the fast-spreading East Pacific Rise (which has a peak contribution at degree and order 9).

IMPLICATIONS FOR THE LITHOSPHERIC REFERENCE STATE

Neglecting local flexural effects, the distribution of stress within continents is a function of tectonic forces acting along the plate boundaries, tractions acting along the base of the plate, and intraplate variations in the lithospheric GPE which set up force gradients across the continents and between continents and adjacent ocean basins (Coblentz et al., 1994; Lithgow-Bertelloni and Guynn, 2004; Heidbach et al., 2010; Ghosh et al., 2009). Because the upper mantle geoid is influenced by density gradients both within the lithosphere and in the sub-lithospheric upper mantle (in response to upper mantle convection), it can be used to refine our understanding of the tectonic reference state. The tectonic reference state is defined as the lithospheric structure that is in potential energy balance with the GPE mean. Thus, the difference between the potential energy (and the geoid) of a lithospheric column and the reference state determines whether the column is in an extensional, neutral, or compressional state of stress. Originally, the close correspondence between the mean GPE of the continents and that of the mid-ocean ridges (Dahlen, 1981; Doin and Fleitout, 1996; Doin et al., 1996) was used to define the reference lithospheric density column and evaluate the "ambient stress" state within plates (Coblentz and Sandiford, 1994).

In addition, because the mid-ocean ridges inherently have little strength, they provide a useful reference frame for the neutral stress state within plates. The observation that the average upper mantle geoid anomaly of continental cratonic regions is near zero (~0.29 m) suggests that in the absence of other tectonic forces (e.g., ambient conditions), the continental in situ stress state will be close to neutral. This is confirmed in the case of Africa, where the average s_1 in the continental regions is observed to be near neutral (2 MPa, ± 3MPa). It has often been assumed that the reference continental lithosphere is in potential energy balance with the mid-ocean ridges (e.g., Turcotte, 1983; Crough, 1983), and elevated continental lithosphere is observed to exceed the potential energy of the mid-ocean ridges (Fig. 2B). Establishing the elevation of a deformed lithospheric column (relative to the lithospheric structure of the reference column) has long been a subject of great interest (Sandiford and Powell, 1990), and evaluation of the upper mantle geoid provides a way to revisit this issue. Plotting the upper mantle geoid anomaly as a function of the elevation of the continental lithosphere (Fig. 8) indicates that continental lithosphere with an elevation of ~750 m is in geoid (and potential energy) balance with the mid-ocean ridges. This relationship suggests that continental regions with an elevation greater than a

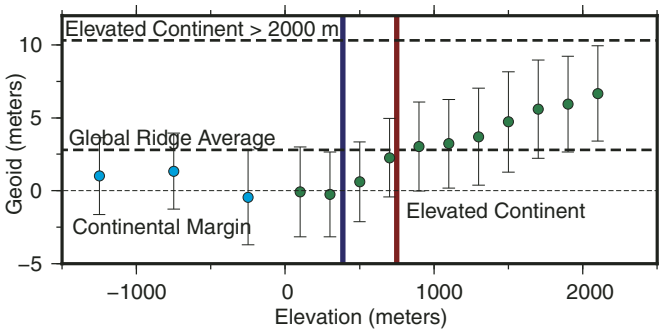

Figure 8. Average global upper mantle geoid anomaly for continental lithosphere plotted as a function of elevation. The average geoid was computed for a ±100 m elevation window about each elevation point (5 arc-minute spatial resolution); error bars are ±1σ about the mean. Blue- and green-filled circles are continental margin and elevated continental locations, respectively. Bold dashed lines designate the global geoid anomaly average (~3 m) for cooling oceanic lithosphere younger than 10 m.y. (which defines the young ridge segments) and the average geoid for elevated continental lithosphere greater than 2000 m elevation (10.1 m). The vertical blue and red lines designate the elevation values for continental lithosphere corresponding to a zero geoid anomaly (~350 m) and the geoid anomaly for the global ridge average (~750 m), respectively.

few hundred meters will be in a state of deviatoric tectonic extension, which is consistent with recent evaluations of the intraplate stress field (Zoback and Mooney, 2003). It should be noted that the elevation of continental lithosphere in potential energy balance with the mid-ocean ridges derived using the upper mantle geoid is in good agreement with the elevation estimates (~940 m) derived using a first-order Airy isostatic model (Coblentz et al., 1994). The fact that two independent approaches arrive at very similar crustal elevation estimates for the reference lithospheric column argues favorably for the robustness of our conclusions.

DISCUSSION

In this contribution, we have exploited the relationship between the geoid and GPE to evaluate and refine our estimates of the lithospheric stress state. Using filtering to extract the upper mantle geoid, we are able to evaluate lithospheric and upper mantle influences on the stress field. This approach allows us to revise estimates of the mean potential energy state of the lithosphere, which heretofore have been based on an assumption of Airy compensation (e.g., Coblentz et al., 1994). We confirm the near-neutral state of stress for stable continental lithosphere with elevations less than a few hundred meters and the geoid equivalence of continental lithosphere with an elevation of 750 m with the mid-ocean ridges. This latter equivalence has important tectonic implications. Because variations in GPE are a principal contributor to the intraplate stress field and lithospheric deformation seeks relaxation of deviatoric stresses, it has been argued (Sandiford, 2010) that the structure of typical undeformed continental lithosphere (surface elevation of around 0.5–1 km above sea level, average crustal thickness of ~40 km, and a total lithospheric thickness of ~125 km) is not a fortuitous geometry but rather the result of a potential energy "attractor state" for the continental lithosphere. In this framework, the potential energy balance between the continents and the mean potential energy of the oceanic ridges drives continents to this average (or reference) structure. Our confirmation that continental lithosphere with an elevation of ~750 m is in potential energy balance with the global average of geoid anomalies associated with ridges lends credibility to this hypothesis and argues favorably that the mean ambient stress state in the continents is tuned to the stress state of the mid-ocean ridges. In aggregate, the results and discussion above support the notion that the Earth's tectonic plates are best viewed as "active" rather than "passive" entities. In the original plate tectonics paradigm, the plates were passive, driven by external forces with deformation limited to their edges. It is our conclusion that a better view is one in which the plates are active in the sense that the plate themselves are actively involved in the generation of the forces controlling the intraplate stress field (in the form of potential energy variations) and accommodation of the resulting strain field as manifested by the "attractor" state of the reference lithospheric geometry. Within Don Anderson's framework of "top-down tectonics", our results support the notion that "shallow" density variations in the upper mantle have a strong correlation with many surface tectonic features and have an important influence on the intraplate stress field.

ACKNOWLEDGMENTS

A number of people have contributed suggestions and ideas to this project. Discussions with members of the CREST (Colorado Rockies Experiment and Seismic Transects) working group have been particularly fruitful. This work was supported by The Institute of Geophysics, Planetary Physics, and Signatures at Los Alamos National Laboratory and by National Science Foundation grant EAR-0607808 (for CREST members). Generic Mapping Tools software (Wessel and Smith, 1991) was used both for the analysis and the figures. Simon Holmes and Nikolaos Pavlis are thanked for their help with modifying the harmonic synthesis code used for the analysis. Constructive comments by two anonymous reviewers helped strengthen this contribution. We also appreciate the constructive comments by Scott King, one of the editors for this volume. This contribution is LANL publication LA-UR-12-10001.

REFERENCES CITED

Allan, R.R., 1972, Depth sources of gravity anomalies: Nature, v. 236, p. 22–23, doi:10.1038/physci236022a0.

Anderson, D.L., 1982, Hotspots, polar wander, Mesozoic convection, and the geoid: Nature, v. 297, p. 391–393, doi:10.1038/297391a0.

Anderson, D.L., 2001, Top-down tectonics?: Science, v. 293, p. 2016–2018, doi:10.1126/science.1065448.

Anderson, D.L., and Schramm, K.A., 2005, Global hotspot maps, *in* Foulger, G.R., Natland, J.H., Presnall, D.C., and Anderson, D.L., eds., Plates, Plumes, and Paradigms: Geological Society of America Special Paper 388, p. 19–29, doi:10.1130/0-8137-2388-4.19.

Artyushkov, E.V., 1973, Stresses in the lithosphere caused by crustal thickness inhomogeneities: Journal of Geophysical Research, v. 78, p. 7675–7708, doi:10.1029/JB078i032p07675.

Becker, T.W., and Boschi, L., 2002, A comparison of tomographic and geodynamic mantle models: Geochemistry Geophysics Geosystems, v. 3, 1003, doi:10.1029/2001GC000168.

Bird, P., Ben-Avraham, Z., Schubert, G., Andreoli, M., and Viola, G., 2006, Patterns of stress and strain rate in southern Africa: Journal of Geophysical Research, v. 111, B08402, doi:10.1029/2005JB003882.

Bowin, C., 1983, Depth of principal mass anomalies contributing to the Earth's geoidal undulations and gravity anomalies: Marine Geodesy, v. 7, p. 61–100, doi:10.1080/15210608309379476.

Bowin, C., 1986, Topography at the core-mantle boundary: Geophysical Research Letters, v. 13, p. 1513–1516, doi:10.1029/GL013i013p01513.

Bowin, C., 2000a, Mass anomalies and the structure of the Earth: Physics and Chemistry of the Earth, Part A: Solid Earth and Geodesy, v. 25, p. 343–353, doi:10.1016/S1464-1895(00)00056-9.

Bowin, C., 2000b, Mass anomaly structure of the Earth: Reviews of Geophysics, v. 38, p. 355–387, doi:10.1029/1999RG000064.

Brown, M., and Rushmer, T., 2006, Evolution and Differentiation of the Continental Crust: Cambridge, UK, Cambridge University Press, 553 p.

Buiter, S.J.H., Steinberger, B., Medvedev, S., and Tetreault, J., 2012, Could the mantle have caused subsidence of the Congo Basin?: Tectonophysics, v. 514–517, p. 62–80, doi:10.1016/j.tecto.2011.09.024.

Burke, K., Steinberger, B., Torsvik, T.H., and Smethurst, M.A., 2008, Plume generation zones at the margins of large low shear velocity provinces on the core-mantle boundary: Earth and Planetary Science Letters, v. 265, p. 49–60, doi:10.1016/j.epsl.2007.09.042.

Cao, Q., van der Hilst, R.D., de Hoop, M.V., and Shim, S.H., 2011, Seismic imaging of transition zone discontinuities suggests hot mantle west of Hawaii: Science, v. 332, p. 1068–1071, doi:10.1126/science.1202731.

Chapman, M.E., 1979, Techniques for interpretation of geoid anomalies: Journal of Geophysical Research, v. 84, p. 3793–3801, doi:10.1029/JB084iB08p03793.

Chase, C.G., 1979, Subduction, the geoid, and lower mantle convection: Nature, v. 282, p. 464–468, doi:10.1038/282464a0.

Chase, C.G., 1985, The geological significance of the geoid: Annual Review of Earth and Planetary Sciences, v. 13, p. 97–117, doi:10.1146/annurev.ea.13.050185.000525.

Chase, C.G., Libarkin, J.A., and Sussman, A.J., 2002, Colorado Plateau: Geoid and means of isostatic support: International Geology Review, v. 44, p. 575–587, doi:10.2747/0020-6814.44.7.575.

Coblentz, D., and Sandiford, M., 1994, Tectonic stresses in the African plate: Constraints on the ambient lithospheric stress state: Geology, v. 22, p. 831–834, doi:10.1130/0091-7613(1994)022<0831:TSITAP>2.3.CO;2.

Coblentz, D., Richardson, R.M., and Sandiford, M., 1994, On the gravitational potential of the Earth's lithosphere: Tectonics, v. 13, p. 929–945, doi:10.1029/94TC01033.

Coblentz, D., Libarkin, J.C., Chase, C.G., and Sussman, A.J., 2007, Paleolithospheric structure revealed by continental geoid anomalies: Tectonophysics, v. 443, p. 106–120, doi:10.1016/j.tecto.2007.06.003.

Coblentz, D., Chase, C.G., Karlstrom, K.E., and van Wijk, J.W., 2011, Topography, the geoid, and compensation mechanisms for the southern Rocky Mountains: Geochemistry Geophysics Geosystems, v. 12, Q04002, p. doi:10.1029/2010GC003459.

Craig, T.J., Jackson, J.A., Priestley, K., and McKenzie, D., 2011, Earthquake distribution patterns in Africa: Their relationship to variations in lithospheric and geological structure, and their rheological implications: Geophysical Journal International, v. 185, p. 403–434, doi:10.1111/j.1365-246X.2011.04950.x.

Crosby, A.G., Fishwick, S., and White, N., 2010, Structure and evolution of the intracratonic Congo Basin: Geochemistry Geophysics Geosystems, v. 11, Q06010, doi:10.1029/2009GC003014.

Crough, S.T., 1979, Hotspot epeirogeny: Tectonophysics, v. 61, p. 321–333, doi:10.1016/0040-1951(79)90304-4.

Crough, S.T., 1983, Rifts and swells: Geophysical constraints on causality: Tectonophysics, v. 94, p. 23–37, doi:10.1016/0040-1951(83)90007-0.

Crough, S.T., and Jurdy, D.M., 1980, Subducted lithosphere, hotspots, and the geoid: Earth and Planetary Science Letters, v. 48, p. 15–22, doi:10.1016/0012-821X(80)90165-X.

Crow, R., Karlstrom, K., Asmerom, Y., Schmandt, B., Polyak, V., and DuFrane, S.A., 2011, Shrinking of the Colorado Plateau via lithospheric mantle erosion: Evidence from Nd and Sr isotopes and geochronology of Neogene basalts: Geology, v. 39, p. 27–30, doi:10.1130/G31611.1.

Cserepes, L., Christensen, U.R., and Ribe, N.M., 2000, Geoid height versus topography for a plume model of the Hawaiian swell: Earth and Planetary Science Letters, v. 178, p. 29–38, doi:10.1016/S0012-821X(00)00065-0.

Dahlen, F.A., 1981, Isostasy and the ambient state of stress in the oceanic lithosphere: Journal of Geophysical Research, v. 86, p. 7801–7807, doi:10.1029/JB086iB09p07801.

Delvaux, D., and Barth, A., 2010, African stress pattern from formal inversion of focal mechanism data: Tectonophysics, v. 482, p. 105–128, doi:10.1016/j.tecto.2009.05.009.

Doin, M.P., and Fleitout, L., 1996, Thermal evolution of the oceanic lithosphere: An alternative view: Earth and Planetary Science Letters, v. 142, p. 121–136, doi:10.1016/0012-821X(96)00082-9.

Doin, M.P., Fleitout, L., and McKenzie, D., 1996, Geoid anomalies and the structure of continental and oceanic lithospheres: Journal of Geophysical Research, v. 101, p. 16,119–16,135, doi:10.1029/96JB00640.

Downey, N.J., and Gurnis, M., 2009, Instantaneous dynamics of the cratonic Congo basin: Journal of Geophysical Research, v. 114, B06401, doi:10.1029/2008JB006066.

Ebbing, J., Braitenberg, C., and Gotze, H.J., 2001, Forward and inverse modelling of gravity revealing insight into crustal structures of the Eastern Alps: Tectonophysics, v. 337, p. 191–208, doi:10.1016/S0040-1951(01)00119-6.

England, P.C., and Houseman, G.A., 1988, The mechanics of the Tibetan Plateau: Philosophical Transactions of the Royal Society of London, Series A: Mathematical Physical and Engineering Sciences, v. 326, p. 301–320, doi:10.1098/rsta.1988.0089.

Featherstone, W.E., 1997, On the use of the geoid in geophysics: A case study over the north-west shelf of Australia: Exploration Geophysics, v. 28, p. 52–57, doi:10.1071/EG997052.

Fleitout, L., and Froidevaux, C., 1983, Tectonics stress in the lithosphere: Tectonics, v. 2, p. 315–324, doi:10.1029/TC002i003p00315.

Fleitout, L., and Froidevaux, C., 1982, Tectonics and topography for a lithosphere containing density heterogeneities: Tectonics, v. 1, p. 21–56, doi:10.1029/TC001i001p00021.

Forte, A.M., and Mitrovica, J.X., 2001, Deep-mantle high-viscosity flow and thermochemical structure inferred from seismic and geodynamic data: Nature, v. 410, p. 1049–1056, doi:10.1038/35074000.

Forte, A.M., Moucha, R., Simmons, N.A., Grand, S., and Mitrovica, J.X., 2010, Deep-mantle contributions to the surface dynamics of the North American continent: Tectonophysics, v. 481, p. 3–15, doi:10.1016/j.tecto.2009.06.010.

Frank, P.C., 1972, Plate tectonics, the analogy with glacier flow, and isostasy, *in* Heard, H.C., Borg, I.Y., Carter, N.L., and Raleigh, C.B., eds., Flow and Fracture of Rocks: Washington, D.C., American Geophysical Union, doi.1029/GM016p0285.

French, S., Lekic, V., and Romanowicz, B., 2013, Waveform tomography reveals channeled flow at the base of the oceanic asthenosphere: Science, v. 342, p. 227–230, doi:10.1126/science.1241514.

Ghosh, A., Holt, W.E., and Flesch, L.M., 2009, Contribution of gravitational potential energy differences to the global stress field: Geophysical Journal International, v. 179, p. 787–812, doi:10.1111/j.1365-246X.2009.04326.x.

Grose, C.J., and Afonso, J.C., 2013, Comprehensive plate models for the thermal evolution of oceanic lithosphere: Geochemistry Geophysics Geosystems, v. 14, p. 3751–3778, doi:10.1002/ggge.20232.

Hager, B.H., 1983, Global isostatic geoid anomalies for plate and boundary layer models of the lithosphere: Earth and Planetary Science Letters, v. 63, p. 97–109, doi:10.1016/0012-821X(83)90025-0.

Hager, B.H., and Richards, M.A., 1989, Long-wavelength variations in Earth's geoid: Physical models and dynamical implications: Philosophical Transactions of the Royal Society of London A, v. 328, p. 309–327, doi:10.1098/rsta.1989.0038.

Hager, B.H., Clayton, R.W., Richards, M.A., Comer, R.P., and Dziewonski, A.M., 1985, Lower mantle heterogeneity, dynamic topography, and the geoid: Nature, v. 313, p. 541–545, doi:10.1038/313541a0.

Haxby, W.F., and Turcotte, D.L., 1978, Isostatic geoid anomalies: Journal of Geophysical Research, v. 83, p. 5473–5478, doi:10.1029/JB083iB11p05473.

Heidbach, O., Tingay, M., Barth, A., Reinecker, J., Kurfess, D., and Muller, B., 2010, Global crustal stress pattern based on the World Stress Map database release 2008: Tectonophysics, v. 482, p. 3–15, doi:10.1016/j.tecto.2009.07.023.

Houseman, G., and England, P., 1986, Finite strain calculations of continental deformation 1. Method and general results for convergent zones: Journal of Geophysical Research, v. 91, doi:10.1029/JB091iB03p03651.

Houseman, G., McKenzie, D., and Molnar, P., 1981, Convective instability of a thickened boundary layer and its relevance for the thermal evolution of continental convergence zones: Journal of Geophysical Research, v. 86, p. 6115–6132, doi:10.1029/JB086iB07p06115.

Humphreys, E., and Coblentz, D., 2007, North American dynamics and western U.S. tectonics: Reviews of Geophysics, v. 45, RG3001, doi:10.1029/2005RG000181.

Hyndman, R.D., and Currie, C.A., 2011, Why is the North American cordillera high? Hot backarcs, thermal isostasy, and mountain belts: Geology, v. 39, p. 783–786, doi:10.1130/G31998.1.

Jones, C.H., Unruh, J.R., and Sonder, L.J., 1996, The role of gravitational potential energy in active deformation in the southwestern United States: Nature, v. 381, p. 37–41, doi:10.1038/381037a0.

Kadima, E., Delvaux, D., Sebagenzi, S.N., Tack, L., and Kabeya, S.M., 2011, Structure and geological history of the Congo Basin: An integrated interpretation of gravity, magnetic and reflection seismic data: Basin Research, v. 23, p. 499–527, doi:10.1111/j.1365-2117.2011.00500.x.

Karlstrom, K.E., Crow, R.S., Peters, L., McIntosh, W., Raucci, J., Crossey, L.J., Umhoefer, P., and Dunbar, N., 2007, $^{40}Ar/^{39}Ar$ and field studies of Quaternary basalts in Grand Canyon and model for carving Grand Canyon: Quantifying the interaction of river incision and normal faulting across the western edge of the Colorado Plateau: Geological Society of America Bulletin, v. 119, p. 1283–1312, doi:10.1130/0016-7606(2007)119[1283:AAFSOQ]2.0.CO;2.

Karlstrom, K.E., Crow, R., Crossey, L.J., Coblentz, D., and Van Wijk, J.W., 2008, Model for tectonically driven incision of the younger than 6 Ma Grand Canyon: Geology, v. 36, p. 835–838, doi:10.1130/G25032A.1.

Karlstrom, K.E., 23 others, and the CREST Working Group., 2012, Mantle-driven dynamic uplift of the Rocky Mountains and Colorado Plateau

and its surface response: Toward a unified hypothesis: Lithosphere, v. 4, p. 3–22, doi:10.1130/L150.1.

Kaula, W.M., 1967, Geophysical implications of satellite determinations of the earth's gravitational field: Space Science Reviews, v. 7, p. 769–794, doi:10.1007/BF00542895.

Kahn, M.A., 1977, Depth sources of gravity anomalies: Geophysical Journal of the Royal Astronomical Society, v. 48, p. 197–209, doi:10.1111/j.1365-246X.1977.tb01296.x.

King, S.D., 1995, The viscosity structure of the mantle: Reviews of Geophysics, v. 33, p. 11–17, doi:10.1029/95RG00279.

King, S.D., and Adam, C., 2014, Hotspot swells revisited: Physics of the Earth and Planetary Interiors, v. 235, p. 66–83, doi:10.1016/j.pepi.2014.07.006.

King, S.D., and Masters, G., 1992, An inversion for radial viscosity structure using seismic tomography: Geophysical Research Letters, v. 19, p. 1551–1554, doi:10.1029/92GL01700.

Lambeck, K., 1988, Geophysical Geodesy: The Slow Deformations of the Earth: Oxford and New York, Oxford University Press, 727 p.

Laske, G., and Masters, G., 1997, A global digital map of sediment thickness [abs.]: Eos (Transactions, American Geophysical Union), v. 78, p. F483.

Levander, A., Schmandt, B., Miller, M.S., Liu, K., Karlstrom, K.E., Crow, R.S., Lee, C.T.A., and Humphreys, E.D., 2011, Continuing Colorado plateau uplift by delamination-style convective lithospheric downwelling: Nature, v. 472, p. 461–465, doi:10.1038/nature10001.

Li, C., van der Hilst, R.D., Engdahl, E.R., and Burdick, S., 2008, A new global model for P wave speed variations in Earth's mantle: Geochemistry Geophysics Geosystems, v. 9, Q05018, doi:10.1029/2007GC001806.

Lister, C.R., 1975, Gravitational drive on oceanic plates caused by thermal contraction: Nature, v. 257, p. 663–665, doi:10.1038/257663a0.

Lithgow-Bertelloni, C., and Guynn, J.H., 2004, Origin of the lithospheric stress field: Journal of Geophysical Research, v. 109, B01408, doi:10.1029/2003JB002467.

Lithgow-Bertelloni, C., and Silver, P.G., 1998, Dynamic topography, plate driving forces and the African superswell: Nature, v. 395, p. 269–272, doi:10.1038/26212.

Liu, K.J., Levander, A., Niu, F.L., and Miller, M.S., 2011, Imaging crustal and upper mantle structure beneath the Colorado Plateau using finite frequency Rayleigh wave tomography: Geochemistry Geophysics Geosystems, v. 12, Q07001, doi:10.1029/2011GC003611.

Liu, L.J., and Gurnis, M., 2010, Dynamic subsidence and uplift of the Colorado Plateau: Geology, v. 38, p. 663–666, doi:10.1130/G30624.1.

Marks, K.M., and Sandwell, D.T., 1991, Analysis of geoid height versus topography for oceanic plateaus and swells using nonbiased linear regression: Journal of Geophysical Research, v. 96, p. 8045–8055, doi:10.1029/91JB00240.

McKenzie, D., Jackson, J., and Priestley, K., 2005. Thermal structure of oceanic and continental lithosphere: Earth and Planetary Science Letters, v. 233, p. 337–349, doi:10.1016/j.epsl.2005.02.005.

Mishra, D.C., and Kumar, M.R., 2012, Long and short wavelengths of Indian Ocean geoid and gravity lows: Mid-to-upper mantle sources, rapid drift and seismicity of Kachchh and Shillong plateau, India: Journal of Asian Earth Sciences, v. 60, p. 212–224, doi:10.1016/j.jseaes.2012.08.024.

Mitrovica, J.X., and Forte, A.M., 1997, The radial profile of mantle viscosity: Results from the joint inversion of convection and post-glacial rebound observables: Journal of Geophysical Research, v. 102, p. 2751–2769, doi:10.1029/96JB03175.

Molnar, P., and Tapponier, P., 1978, Active tectonics of Tibet: Journal of Geophysical Research, v. 83, p. 5361–5375, doi:10.1029/JB083iB11p05361.

Montelli, R., Nolet, G., Dahlen, F.A., Masters, G., Engdahl, R., and Hung, S., 2004, Finite-frequency tomography reveals a variety of plumes in the mantle: Science, v. 303, p. 338–343, doi:10.1126/science.1092485.

Moucha, R., and Forte, A.M., 2011, Changes in African topography driven by mantle convection: Nature Geoscience, v. 4, p. 707–712, doi:10.1038/ngeo1235.

Moucha, R., Forte, A.M., Rowley, D.B., Mitrovica, J.X., Simmons, N.A., and Grand, S.P., 2009, Deep mantle forces and the uplift of the Colorado Plateau: Geophysical Research Letters, v. 36, L19310, doi:10.1029/2009GL039778.

Naliboff, J.B., Conrad, C.P., and Lithgow-Bertelloni, C., 2009, Modification of the lithospheric stress field by lateral variations in plate-mantle coupling: Geophysical Research Letters, v. 36, L22307, doi:10.1029/2009gl040484.

Naliboff, J.B., Lithgow-Bertelloni, C., Ruff, L.J., and de Koker, N., 2011, The effects of lithospheric thickness and density structure on Earth's stress field: Geophysical Journal International, v. 188, p. 1–17, doi:10.1111/j.1365-246X.2011.05248.x.

Ni, S., and Helmberger, D.V., 2003, Seismological constraints of the South African superplume: Could be the oldest distinct structure on Earth: Earth and Planetary Science Letters, v. 206, p. 119–131, doi:10.1016/S0012-821X(02)01072-5.

Parsons, B., and Sclater, J.G., 1977, An analysis of the variation of ocean floor bathymetry and heat flow with age: Journal of Geophysical Research, v. 82, p. 803–827, doi:10.1029/JB082i005p00803.

Parsons, T., Thompson, G.A., and Sleep, N.A., 1994, Mantle plume influence on the Neogene uplift and extension of the U.S. western cordillera: Geology, v. 22, p. 83–86, doi:10.1130/0091-7613(1994)022<0083:MPIOTN>2.3.CO;2.

Pavlis, N.K., Holmes, S.A., Kenyon, S.C., and Factor, J.K., 2012, The development and evaluation of the Earth Gravitational Model 2008 (EGM2008): Journal of Geophysical Research, v. 117, B04406, doi:10.1029/2011JB008916.

Prodehl, C., and Mooney, W.D., 2012, Exploring the Earth's Crust: History and Results of Controlled-Source Seismology: Geological Society of America Memoir 208, 764 p., doi:10.1130/9780813712086.

Ricard, Y., Fleitout, L., and Froidevaux, C., 1984, Geoid heights and lithospheric stresses for a dynamic Earth: Annales Geophysicae, v. 2, no. 3, p. 267–286.

Richardson, R.M., and Cox, B.L., 1984, Evolution of oceanic lithosphere: A driving force study of the Nazca Plate: Journal of Geophysical Research, v. 89, p. 10,043–10,052, doi:10.1029/JB089iB12p10043.

Sandiford, M., 2010, Why are the continents just so...?: Journal of Metamorphic Geology, v. 28, p. 569–577, doi:10.1111/j.1525-1314.2010.00888.x.

Sandiford, M., and Coblentz, D., 1994, Plate-scale potential-energy distributions and the fragmentation of aging plates: Earth and Planetary Science Letters, v. 126, p. 143–159, doi:10.1016/0012-821X(94)90247-X.

Sandiford, M., and Powell, R., 1990, Some isostatic and thermal consequences of the vertical strain geometry in convergent orogens: Earth and Planetary Science Letters, v. 98, p. 154–165, doi:10.1016/0012-821X(90)90056-4.

Sandwell, D.T., and Mackenzie, K.R., 1989, Geoid height versus topography for oceanic plateaus and swells: Journal of Geophysical Research, v. 94, p. 7403–7418, doi:10.1029/JB094iB06p07403.

Sandwell, D.T., and Renkin, M.L., 1988, Compensation of swells and plateaus in the North Pacific: No direct evidence for mantle convection: Journal of Geophysical Research, v. 93, p. 2775–2783, doi:10.1029/JB093iB04p02775.

Sandwell, D., and Schubert, G., 1980, Geoid height versus age for symmetric spreading ridges: Journal of Geophysical Research, v. 85, p. 7235–7241, doi:10.1029/JB085iB12p07235.

Sonder, L.J., and Jones, C.H., 1999, Western United States extension: How the west was widened: Annual Review of Earth and Planetary Sciences, v. 27, p. 417–462, doi:10.1146/annurev.earth.27.1.417.

Stamps, D.S., Flesch, L.M., and Calais, E., 2010, Lithospheric buoyancy forces in Africa from a thin sheet approach: International Journal of Earth Sciences, v. 99, p. 1525–1533, doi:10.1007/s00531-010-0533-2.

Stamps, D.S., Flesch, L.M., Calais, E., and Ghosh, A., 2014, Current kinematics and dynamics of Africa and the East African Rift System: Journal of Geophysical Research, v. 119, p. 5161–5186, doi:10.1002/2013JB010717.

Stein, C.A., and Stein, S., 1992, A model for the global variation in oceanic depth and heat flow with lithospheric age: Nature, v. 359, p. 123–129, doi:10.1038/359123a0.

Tian, Y., Sigloch, K., and Nolet, G., 2009, Multiple-frequency SH-wave tomography of the western U.S. upper mantle: Geophysical Journal International, v. 178, p. 1384–1402, doi:10.1111/j.1365-246X.2009.04225.x.

Turcotte, D.L., 1983, Mechanisms of crustal deformation: Journal of the Geologic Society of London, v. 140, p. 701–724, doi:10.1144/gsjgs.140.5.0701.

Turcotte, D.L., and McAdoo, D.C., 1979, Geoid anomalies and the thickness of the lithosphere: Journal of Geophysical Research, v. 84, p. 2381–2387, doi:10.1029/JB084iB05p02381.

Turcotte, D.L., and Oxburgh, E.R., 1967, Finite amplitude convection cells and continental drift: Journal of Fluid Mechanics, v. 28, p. 29–42, doi:10.1017/S0022112067001880.

Turcotte, D.L., and Schubert, G., 2014, Geodynamics: Cambridge, UK, New York, Cambridge University Press, 636 p.

van Wijk, J.W., Baldridge, W.S., van Hunen, J., Goes, S., Aster, R., Coblentz, D.D., Grand, S.P., and Ni, J., 2010, Small-scale convection at the edge

of the Colorado Plateau: Implications for topography, magmatism, and evolution of Proterozoic lithosphere: Geology, v. 38, p. 611–614, doi:10.1130/G31031.1.

Vanicek, P., and Christou, N.T., 1994, Geoid and Its Geophysical Interpretations: Ann Arbor, Michigan, CRC Press, 343 p.

Watts, A.B., Sandwell, D.T., Smith, W.H.F., and Wessel, P., 2006, Global gravity, bathymetry, and the distribution of submarine volcanism through space and time: Journal of Geophysical Research, v. 111, B08408, doi:10.1029/2005jb004083.

Wessel, P., and Smith, W.H., 1991, Free software helps map and display data [abs.]: Eos (Transactions, American Geophysical Union), v. 72, p. 441, doi:10.1029/90EO00319.

Wolfe, C., Solomon, S.C., Laske, G., Collins, J., Detrick, R.S., Orcutt, J.A., Bercovici, D., and Hauri, E., 2009, Mantle shear-wave velocity structure beneath the Hawaiian hot spot: Science, v. 326, p. 1388–1390, doi:10.1126/science.1180165.

Yuan, H., and Dueker, K., 2005, Teleseismic P-wave tomogram of the Yellowstone plume: Geophysical Research Letters, v. 32, L07304, doi:10.1029/2004GL022056.

Zhang, Y., Teng, J., Wang, Q., and Hu, G., 2014, Density structure and isostatic state of the crust in the Longmenshan and adjacent areas: Tectonophysics, v. 619, p. 51–57, doi:10.1016/j.tecto.2013.08.018.

Zhou, S.H., and Sandiford, M., 1992, On the stability of isostatically compensated mountain belts: Journal of Geophysical Research, v. 97, p. 14207–14221, doi:10.1029/92JB01091.

Zoback, M.L., and Mooney, W.D., 2003, Lithospheric buoyancy and continental intraplate stresses: International Geology Review, v. 45, p. 95–118, doi:10.2747/0020-6814.45.2.95.

Manuscript Accepted by the Society 24 February 2015
Manuscript Published Online 4 September 2015

Printed in the USA